Drought Mitigation Center Faculty Publications   Drought -- National Drought Mitigation Center

4-15-2011

Evaluation of Drought Indices Based on Thermal Remote Sensing of Evapotranspiration over the Continental United States

Martha C. Anderson
USDA-ARS, martha.anderson@ars.usda.gov

Christopher R. Hain
University of Alabama in Huntsville, christopher.hain@nasa.gov

Brian Wardlow
University of Nebraska-Lincoln, bwardlow2@unl.edu

Agustin Pimstein
USDA-ARS

John R. Mecikalski
University of Alabama in Huntsville

See next page for additional authors

Follow this and additional works at: https://digitalcommons.unl.edu/droughtfacpub

Part of the Climate Commons, Environmental Indicators and Impact Assessment Commons, Environmental Monitoring Commons, Hydrology Commons, Other Earth Sciences Commons, and the Water Resource Management Commons

Authors

Martha C. Anderson, Christopher R. Hain, Brian Wardlow, Agustin Pimstein, John R. Mecikalski, and William P. Kustas

Evaluation of Drought Indices Based on Thermal Remote Sensing of Evapotranspiration over the Continental United States

MARTHA C. ANDERSON,* CHRISTOPHER HAIN,[+] BRIAN WARDLOW,[#] AGUSTIN PIMSTEIN,*
JOHN R. MECIKALSKI,[+] AND WILLIAM P. KUSTAS*

* *Hydrology and Remote Sensing Laboratory, ARS, USDA, Beltsville, Maryland*
[+] *Department of Atmospheric Science, University of Alabama in Huntsville, Huntsville, Alabama*
[#] *National Drought Mitigation Center, University of Nebraska, Lincoln, Nebraska*

ABSTRACT

The reliability of standard meteorological drought indices based on measurements of precipitation is limited by the spatial distribution and quality of currently available rainfall data. Furthermore, they reflect only one component of the surface hydrologic cycle, and they cannot readily capture nonprecipitation-based moisture inputs to the land surface system (e.g., irrigation) that may temper drought impacts or variable rates of water consumption across a landscape. This study assesses the value of a new drought index based on remote sensing of evapotranspiration (ET). The evaporative stress index (ESI) quantifies anomalies in the ratio of actual to potential ET (PET), mapped using thermal band imagery from geostationary satellites. The study investigates the behavior and response time scales of the ESI through a retrospective comparison with the standardized precipitation indices and Palmer drought index suite, and with drought classifications recorded in the U.S. Drought Monitor for the 2000–09 growing seasons. Spatial and temporal correlation analyses suggest that the ESI performs similarly to short-term (up to 6 months) precipitation-based indices but can be produced at higher spatial resolution and without requiring any precipitation data. Unique behavior is observed in the ESI in regions where the evaporative flux is enhanced by moisture sources decoupled from local rainfall: for example, in areas of intense irrigation or shallow water table. Normalization by PET serves to isolate the ET signal component responding to soil moisture variability from variations due to the radiation load. This study suggests that the ESI is a useful complement to the current suite of drought indicators, with particular added value in parts of the world where rainfall data are sparse or unreliable.

1. Introduction

The U.S. Drought Monitor (USDM), considered to be the current state-of-the art drought monitoring tool for the United States, is developed through expert integration of a diverse set of quantitative drought indicators along with local reports from observers in the field (Svoboda et al. 2002). Multiple indicators are required to track the various types of drought, which include 1) meteorological drought, describing short-term precipitation deficits; 2) agricultural drought, reflecting root-zone soil moisture deficits and impacts on crop yields; 3) hydrologic drought, which affects streamflow, groundwater tables, and reservoir levels, and occurs and recovers over much longer time scales (months to years); and 4) socioeconomic drought, incorporating the concept of water supply and demand (Wilhite and Glantz 1985). Online access to current and historical USDM (http://www.drought.unl.edu/dm/) and drought impact reports (http://droughtreporter.unl.edu/) is provided by the National Drought Mitigation Center (NDMC).

Standard indicators currently used in the USDM focus on different components of the hydrologic budget: precipitation, soil moisture content (and its impact on vegetation condition), groundwater storage, runoff, and streamflow. Together, these indicators provide a diversity of information about current hydrologic conditions. They use different input datastreams, have different time scales of response to moisture deficits, and reflect different environmental and social impacts of drought. This is advantageous because a convergence of evidence from multiple independent indicators provides better confidence in an emerging drought signal.

Corresponding author address: M. C. Anderson, Hydrology and Remote Sensing Lab, Bldg. 007, Rm. 104 BARC-West, 10300 Baltimore Ave., Beltsville, MD 20705.
E-mail: martha.anderson@ars.usda.gov

Most of these standard drought indices require spatially distributed observations of precipitation as a primary input, acquired either through rain gauge networks, Doppler radar estimates, satellite observations, or some combination thereof. Precipitation maps may be used as the sole input for some indices, such as in the standardized precipitation indices (SPIs; McKee et al. 1995), or in combination with other observable quantities, such as satellite-based vegetation cover fraction in the vegetation drought response index (VegDRI; Brown et al. 2008). In other cases, precipitation data are transformed into an indicator of soil moisture using water balance models of varying complexity, ranging from the simple two-layer bucket model used in the Palmer index suite (Palmer 1965) to the more detailed multilayer soil moisture schemes used in land surface models (LSMs) in the North American Land Data Assimilation System (NLDAS; Mitchell et al. 2004).

Precipitation-based indices necessarily rely on the availability of high-quality rainfall data, while soil moisture models additionally require accurate information about moisture depletion rate via transpiration, evaporation, drainage, and horizontal transport. These data requirements present significant challenges for global drought monitoring efforts. While real-time precipitation analyses of reasonable quality are available over most of the United States (e.g., McEnery et al. 2005), many parts of world lack sufficiently dense radar and rain gauge networks. Satellite-derived global precipitation products provide improved spatial coverage (Huffman et al. 2007; Joyce et al. 2004), but they are known to exhibit seasonally and spatially dependent biases (Villarini et al. 2009; Zeweldi and Gebremichael 2009). Drought classifications from prognostic water balance models (e.g., NLDAS) depend strongly on the assumed model physics, dynamic forcings, and subsurface properties (Mo 2008), requiring information about soil-moisture-holding capacity and retention characteristics that is difficult to obtain with adequate accuracy over large areas. Biased specifications of total moisture inputs and soil hydraulic properties can introduce significant cumulative biases into prognostic soil moisture estimates (Schaake et al. 2004).

In this paper we evaluate a new remote sensing evaporative stress index (ESI), representing temporal anomalies in the ratio of actual evapotranspiration (ET) to potential ET (PET). In contrast with precipitation-based indices, the ESI algorithm requires no information about antecedent precipitation or subsurface soil characteristics. In this modeling approach, time-differential land surface temperature (LST) measurements derived from satellite imagery collected by the Geostationary Operational Environmental Satellites (GOES) in the thermal infrared (TIR) atmospheric window channel (~10.7 μm) are combined with shortwave information about vegetation cover fraction to directly diagnose evaporative fluxes at 5–10-km spatial resolution (Anderson et al. 2007c). Because the ESI does not use rainfall data, it provides an independent check on precipitation-based drought indicators and may be more robust in regions with minimal ground-based meteorological infrastructure. The remotely sensed ET fields have the advantage that they inherently include nonprecipitation-related moisture signals that need to be modeled a priori in prognostic LSM schemes.

This paper compares the ESI with standard precipitation-based drought indices over the continental United States, and with drought classifications recorded in retrospective USDM reports from 2000 to 2009. The goals of this study are to establish the level of similarity between ET- and precipitation-based indices, and to improve our understanding of the characteristic time scales associated with these indices and their ability to rank historic drought events in order of severity.

2. Data and methodology

The suite of satellite- and precipitation-based drought indices considered in the intercomparison are listed in Table 1 and described briefly below. The precipitation index datasets were generated by the National Climatic Data Center (NCDC; http://www1.ncdc.noaa.gov/pub/data/cirs/) and are included here to study the comparative behavior of a range in metrics commonly used in operational drought monitoring. A more complete review of standard meteorological drought indices is provided by Heim (2002).

The study was conducted over the continental United States (CONUS) using data from 2000 to 2009, focusing on the primary growing season for most of the United States (April–September). The seasonal extent of the intercomparison is currently constrained by the ESI archive, which to date has excluded months with significant snow cover due to poor performance of satellite insolation products over snow. Ultimately, the ESI archive can be extended back to 1979 using GOES imagery archived through the NCDC International Satellite Cloud Climatology Project (ISCCP) B1 Data Rescue project (Knapp 2008). In comparison, the precipitation-based index datasets examined here extend back to 1895, being independent of satellite data.

Figure 1 shows the cumulative percent area in the United States covered by extremely dry and extremely wet conditions for 1900–2009, as indicated by the Palmer drought severity index (PDSI). In contrast with the full period of record, 2000–09 was relatively dry; but it still shows significant variability in drought conditions.

TABLE 1. Drought indicators included in the intercomparison study.

Index	Acronym	Type
U.S. Drought Monitor	USDM	Multi-index synthesis
Evaporative stress index (X-month composite)	ESI-X	Remote sensing of f_{PET}
Evapotranspiration index (X-month composite)	ETI-X	Remote sensing of ET
Standardized precipitation index (X month)	SPI-X	Precipitation
Palmer Z index	Z	Precipitation + storage
Palmer drought severity index	PDSI	Precipitation + storage
Palmer modified drought index	PMDI	Precipitation + storage
Palmer hydrologic drought index	PHDI	Precipitation + storage

a. Remotely sensed ET indices

1) THE ALEXI MODEL

Two remote sensing drought indicators are examined in this study—anomalies in ET and f_{PET}, which is the ratio of actual ET to PET:

$$f_{PET} = \frac{ET}{PET}, \qquad (1)$$

as determined under clear-sky conditions. In this analysis, ET and PET are instantaneous estimates at shortly before local noon, retrieved using the LST-based Atmosphere–Land Exchange Inverse (ALEXI) surface energy balance model (Anderson et al. 1997; Anderson et al. 2007b,c; Mecikalski et al. 1999). Equation (1) follows from earlier work on using TIR-band data in agricultural applications, where f_{PET} has been used as a tool for crop stress detection and irrigation scheduling (Moran 2003). Limiting the assessment to clear-sky conditions separates signals of soil moisture variability from that of cloud climatology. Furthermore, TIR-band LST retrievals are limited to cloud-free atmospheric conditions.

Normalization by PET in Eq. (1) serves to remove some degree of variability in ET due to seasonal variations in available energy and vegetation cover amount, further refining the focus on the soil moisture signal. The analyses below will assess whether f_{PET} anomalies are more strongly related to precipitation drought indices than are anomalies in ET itself. Standardized anomalies in ET and f_{PET} will be referred to as the evapotranspiration index (ETI) and ESI, respectively.

In remote sensing models like ALEXI, surface radiometric temperature derived from TIR-band imagery is a valuable metric for constraining estimates of ET because varying soil moisture conditions yield a distinctive thermal signature: soil surface temperature increases with decreasing water content in the upper few centimeters of the soil profile, while moisture deficiencies in the root zone lead to vegetation stress and elevated canopy temperature. The land surface representation in the ALEXI model is based on the series version of the local-scale two-source (soil + canopy) energy balance (TSEB) model of Norman et al. (1995), with subsequent modifications described by Kustas and Norman (1999, 2000). LST is used to directly constrain the flux of sensible heat (H; W m^{-2}) from the land surface, and latent heat (λE; W m^{-2}) is computed as a residual to the overall energy balance:

$$\lambda E = RN - G - H, \qquad (2)$$

where RN is net radiation and G is the soil heat conduction flux (both in W m^{-2}), λ is the latent heat of vaporization (J kg^{-1}), and E is actual ET (kg s^{-1} m^{-2} or mm s^{-1}). The two-source formulation specific to TSEB further partitions RN, H and into λE into soil and canopy components, facilitating the separation of ET into estimates of soil evaporation and canopy transpiration. This approach therefore opens the potential for surface
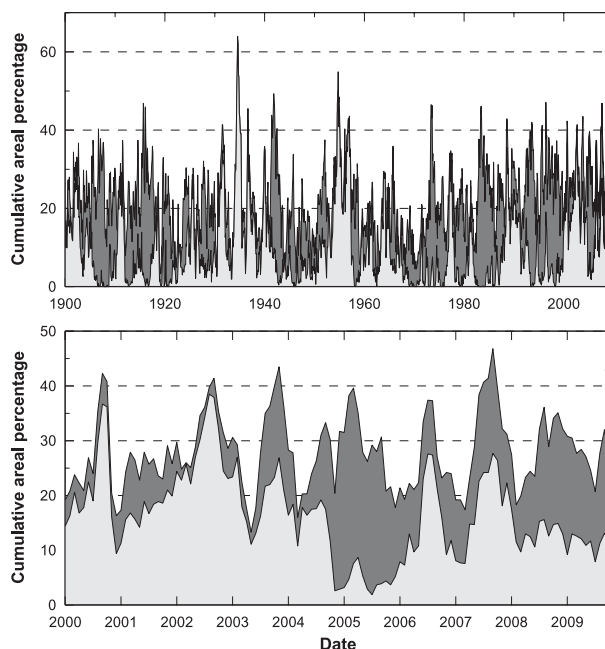

FIG. 1. Cumulative percent area of the United States covered by extremely dry (light gray) and extremely wet (dark gray) conditions for (top) 1900–2009 and (bottom) for the 2000–09 period covered by this analysis, as represented by the PDSI.

and root-zone moisture pool assessment, and thus concomitant tracking of both meteorological and agricultural droughts.

The ALEXI modeling framework enables regional implementation of the TSEB by exploiting the spatial and temporal coverage provided by geostationary satellite platforms, such as GOES in the United States. In the regional ALEXI model, the TSEB is applied in a time-differencing mode, using a simple model of atmospheric boundary layer (ABL) development (McNaughton and Spriggs 1986) to provide energy closure over the integration interval. As a result of this configuration, ALEXI uses only time-differential TIR signals from GOES, thereby reducing flux errors due to absolute sensor calibration and atmospheric and emissivity corrections (Kustas et al. 2001). Anderson et al. (2007a) summarize ALEXI validation experiments, employing a spatial flux disaggregation technique (DisALEXI; Norman et al. 2003), which uses higher-resolution TIR imagery from aircraft or polar-orbiting satellites to downscale the GOES-based flux estimates (10-km resolution) to the flux measurement footprint (on the order of 100 m). Typical root-mean-square deviations in comparison with tower flux measurements (30-min averages) of H and λE are 35–40 W m^{-2} (15% of the mean observed flux) over a range in vegetation cover types and climatic conditions.

The ALEXI model currently runs daily on a 10-km resolution grid covering CONUS, and model input–output from this framework has been archived for the period 2000–present and for the months of February–September. Snow-covered regions have been masked using the 24-km resolution daily Northern Hemisphere snow and ice analysis product distributed through the National Snow and Ice Data Center (NSIDC; http://nsidc.org/data/docs/noaa/g02156_ims_snow_ice_analysis/index.html). Further details about the ALEXI CONUS modeling system are provided by Anderson et al. (2007c).

2) TEMPORAL COMPOSITING

Because the ET values used to compute the ESI and ETI are dependent on clear-sky conditions, only a portion of the ALEXI modeling domain can be filled on any given day. On average, pixels in 75% of the U.S. domain are executed at least once every 6 days, while 95% are updated at least every 20 days. Therefore, temporal compositing of clear-sky ET and f_{PET} values is required to fill in the full model domain. Compositing also serves to reduce the effects of noise in the ET retrievals, primarily arising from incomplete cloud clearing in the LST inputs to ALEXI.

In this study, composites were generated at 28-day time steps (roughly monthly) over 4-, 8-, 12-, and 26-week

(1, 2, 3, and roughly 6 months, respectively) moving windows (time-stamped by the end date), in general paralleling the shorter-term SPI product time scales. The 26-week composite is essentially a growing-season average for April–September, while the 4- to 12-week composites sample different phenological phases in vegetation development. Composites were computed as an unweighted average of all index values over the interval in question that passed cloud screening tests:

$$\langle v(w,y,i,j) \rangle = \frac{1}{\text{nc}} \sum_{n=1}^{\text{nc}} v(n,y,i,j), \qquad (3)$$

where $\langle v(w, y, i, j) \rangle$ is the composite for week w, year y, and i, j grid location; $v(n, y, i, j)$ is the value on day n; and nc is the number of clear days during the compositing interval.

3) STANDARDIZED ANOMALIES

To highlight differences in moisture conditions between years, drought indices are typically presented as anomalies or percentiles with respect to multiyear-average fields determined over some period of record. Standardized anomalies in f_{PET} and ET over the period 2000–09 are expressed as a pseudo z score, normalized to a mean of 0 and a standard deviation of 1. Fields describing "normal" (mean) conditions and temporal standard deviations at each pixel were generated for each compositing interval. Then standardized anomalies were computed as

$$\Delta \langle v(w,y,i,j) \rangle = \frac{\langle v(w,y,i,j) \rangle - \frac{1}{\text{ny}} \sum_{y=1}^{\text{ny}} \langle v(w,y,i,j) \rangle}{\sigma(w,i,j)}, \tag{4}$$

where the second term in the numerator defines the normal field, averaged over all years ny, and the denominator is the standard deviation.

In this notation, ETI-X is defined as $\Delta \langle ET \rangle$ and ESI-X as $\Delta \langle f_{PET} \rangle$, computed for an X-month composite. Like most other drought indices, this formulation generates negative values for drier-than-normal conditions and positive values for wetter-than-normal conditions. Implicit in the application of Eq. (5) to ALEXI ET and f_{PET} is the assumption that these quantities are normally distributed in time at every i, j location in the CONUS grid during 2000–09. In this case, values of ESI and ETI less than -2 represent dry conditions exceeding 2σ, which should occur 2% of the time. At present, there are not enough years in the ALEXI archive (10 points) to warrant fitting of a nonnormal distribution; however, such

adjustments may be applied as the archive is continually expanded.

b. Comparison drought metrics

1) PALMER INDICES

(i) PDSI

The Palmer drought severity index (PDSI; Palmer 1965) was the first drought indicator developed for the United States. Despite its limitations, it is still one of the most widely used indicators today. The algorithm computes a simple two-layer soil water balance equating change in soil water storage with precipitation less ET and runoff terms. Monthly precipitation is compared to a value required to sustain a normal or ''climatically appropriate'' water balance for that month (as determined from precipitation and temperature data acquired over a long period of record), and this departure is weighted to form a Z index (or moisture anomaly index). The weighting factor incorporates local climatic norms for the water balance terms and is intended to improve the comparability of index values over space and time. The Z indices are then accumulated over time using a recursive relationship:

$$PDSI = 0.897 PDSI_{i-1} + \left(\frac{1}{3}\right) Z_i, \qquad (5)$$

where i represents the ith month of a dry spell. The relative contribution from the previous month's PDSI in relationship to the current month's Z index was determined empirically by Palmer using a set of drought events of specified severity and duration that were recorded in central Iowa and western Kansas. Additional rules modify the accumulation of PDSI in Eq. (5) depending on whether a location is in an incipient or existing dry or wet spell, with the end point of a drought not detected until several months or years later. This necessitates backtracking and recomputation of PDSI once a spell has been determined to have been terminated, which can result in sudden temporal discontinuities in the PDSI record.

The inputs to the Palmer algorithm are air temperature (used in ET computation, generally using a Thornthwaite approximation for PET; Thornthwaite 1948), precipitation, and a map of soil available water capacity (related to soil texture). Because of the high weighting of $PDSI_{i-1}$ relative to Z_i, the index has been shown to have a relatively long memory of antecedent moisture conditions, and therefore it is less effective with short-term droughts.

(ii) PMDI

To facilitate the real time, operational application of the PDSI, Heddinghaus and Sabol (1991) modified the

rules of accumulation during wet and dry spells to create the Palmer modified drought index (PMDI). These redefinitions circumvent the need to backtrack and recompute prior PDSI values, as stipulated by the rules of Palmer (1965).

(iii) Z

The Palmer Z index is the Z component of the PDSI computation [Eq. (5)], reflecting the monthly departure in precipitation (supply) with respect to expected demand for that month, as determined by the Palmer soil water balance model. Because Z is not influenced by the moisture conditions from the previous month, it is effectively a measure of short-term meteorological drought.

(iv) PHDI

The Palmer hydrological drought index (PHDI) is also derived as an intermediate index in the PDSI computation, and it represents accumulations derived during an established wet or dry spell. The rules for terminating a dry or wet spell are more stringent than for the PDSI; therefore, the time constant for variation is longer. The PHDI is therefore considered a measure of long-term hydrologic drought.

(v) Summary

The principle advantages of the Palmer indices are a long period of record and a long history of usage, both of which have fostered familiarity within the drought community. Specific limitations of the Palmer indices are reviewed by Alley (1984) and Karl (1983). Because the algorithm is highly parameterized, with empirically based parameter values determined from limited observational data exclusively from the midwestern United States, there are issues with spatial and temporal standardization (Wells et al. 2004). The ET and two-layer soil storage model components are simplistic and depend on accurate soil texture information. Finally, given the complex algorithm applied, Palmer index values have no directly intuitive physical meaning.

Palmer datasets Z, PDSI, PMDI, and PDHI are distributed by NCDC at the climate division level and on a monthly time step from 1895 to present (http://www1.ncdc.noaa.gov/pub/data/cirs/). These products are based on rain gauge and air temperature data that have been area averaged at the climate division scale (Guttman and Quayle 1996). For this study, the Palmer datasets were regridded to the 10-km ALEXI grid, maintaining constant values over climate division polygons.

2) SPI

Issues with PDSI and variants thereof inspired the formation of a standardized precipitation index (SPI;

McKee et al. 1993, 1995), which uses observed precipitation as its only input. Precipitation data at a given location are converted into probabilities based on a local long-term climatology. The probabilities are then standardized such that a value of 0 indicates that the median precipitation amount (in comparison with the climatology) was measured at that pixel over the time interval in question (Edwards and McKee 1997). The SPI can be computed for multiple time scales (typically ranging from 2 to 52 weeks) to monitor the different types of drought.

The advantage of the SPI is that it is model independent—a straight forward assessment of rainfall inputs to the system, unlike the Palmer indices, which make assumptions about water loss and storage as noted above. Spatial uniformity and time scale of the SPI are well defined, (Guttman 1997). Because it is based only on precipitation data, a long period of record spanning many decades can be constructed. A major disadvantage of the SPI (and the Palmer indices) for mapping applications is that high-quality gridded precipitation data are not available at high spatial resolution for most parts of the world.

SPI data are distributed by NCDC at the climate division level and on a monthly time step from 1895 to present (http://www1.ncdc.noaa.gov/pub/data/cirs/). These products are based on rain gauge data areal averaged at the climate division scale. In this study we evaluate the 2-, 3-, and 6-month NCDC SPI products. Longer-term SPI products (e.g., 9 and 12 months) extend beyond the annual growing-season extent of the current ESI archive and will be assessed in a future study when the archive has been expanded to year-round coverage. The SPI datasets were regridded to the 10-km ALEXI grid, maintaining constant values over climate division polygons.

3) USDM

Through expert analysis, authors of the weekly USDM subjectively integrate information from many existing drought indicators, including the Palmer indices and the SPI, along with local reports from state climatologists and observers across the country. Archived USDM data are distributed by the NDMC online (http://drought.unl.edu/dm/) in a variety of GIS formats. In this study, USDM data were downloaded in table form, which indexes the percent areas of each USDM drought class by calendar date and county.

County polygons were used to assign a USDM value for each date to each pixel in the 10-km ALEXI grid. All pixels contained within a given county polygon were assigned the same value, corresponding to the most severe drought class observed over at least 33% of the county. For computational purposes, the drought classes

were mapped to numerical values with "no drought" assigned a value of -1, D0 = 0 (abnormally dry), D1 = 1 (moderate drought), D2 = 2 (severe drought), D3 = 3 (extreme drought), and D4 = 4 (exceptional drought). For example, if a particular county were classified as 100% D0, 38% D1, and 0% D2–D4, the pixels in that county would be assigned a value of 1.

4) STANDARDIZED ANOMALIES

The PDSI and SPI data used here were normalized by the NCDC to the period 1931–90. The period of record for the ESI and ETI (2000–09) is considerably shorter, with average climatic conditions that are not necessarily representative of the normalization periods for the other indices (Fig. 1). Therefore, the terms "wetter" and "drier" may convey different meaning for the ESI than for the PDSI and SPI. To improve the comparability between the indices evaluated here, anomalies for each precipitation-based index included in the intercomparison and for the USDM drought classes were recomputed over the period 2000–09 using Eq. (4), analogous to the ESI formulation. Recomputation of anomalies with respect to the same period of record significantly improved the spatial agreement between indices. Renormalized values of index X will be referred to as "ΔX" to distinguish them from their standard values.

c. Statistical comparisons

Both temporal and spatial correlations between index anomalies were examined to assess the similarity between drought indices in their ability to rank drought severity and to visualize spatial patterns in index congruity. For these statistical analyses, all index anomaly maps were aggregated to the climate division scale, which was the scale of the coarsest indices included in the intercomparison.

First, we examined temporal correlations between drought indices and the USDM—that is, how similarly these indicators rank drought conditions through time at a given point in space. In this case, index time series were extracted from six monthly maps per year, yielding a total of $6 \times 10 = 60$ data pairs in the correlation computation at each point in the modeling domain. The Pearson correlation coefficient was then mapped as a function of location across CONUS. A Spearman rank correlation test was also applied, but it gave similar results.

We also examined the spatial similarity between index maps to determine how uniformly and consistently drought events were classified over CONUS by this suite of indicators at different points in time. Correlation coefficients for each month (April–September) for 2000–09 were computed between pixels from pairs of index
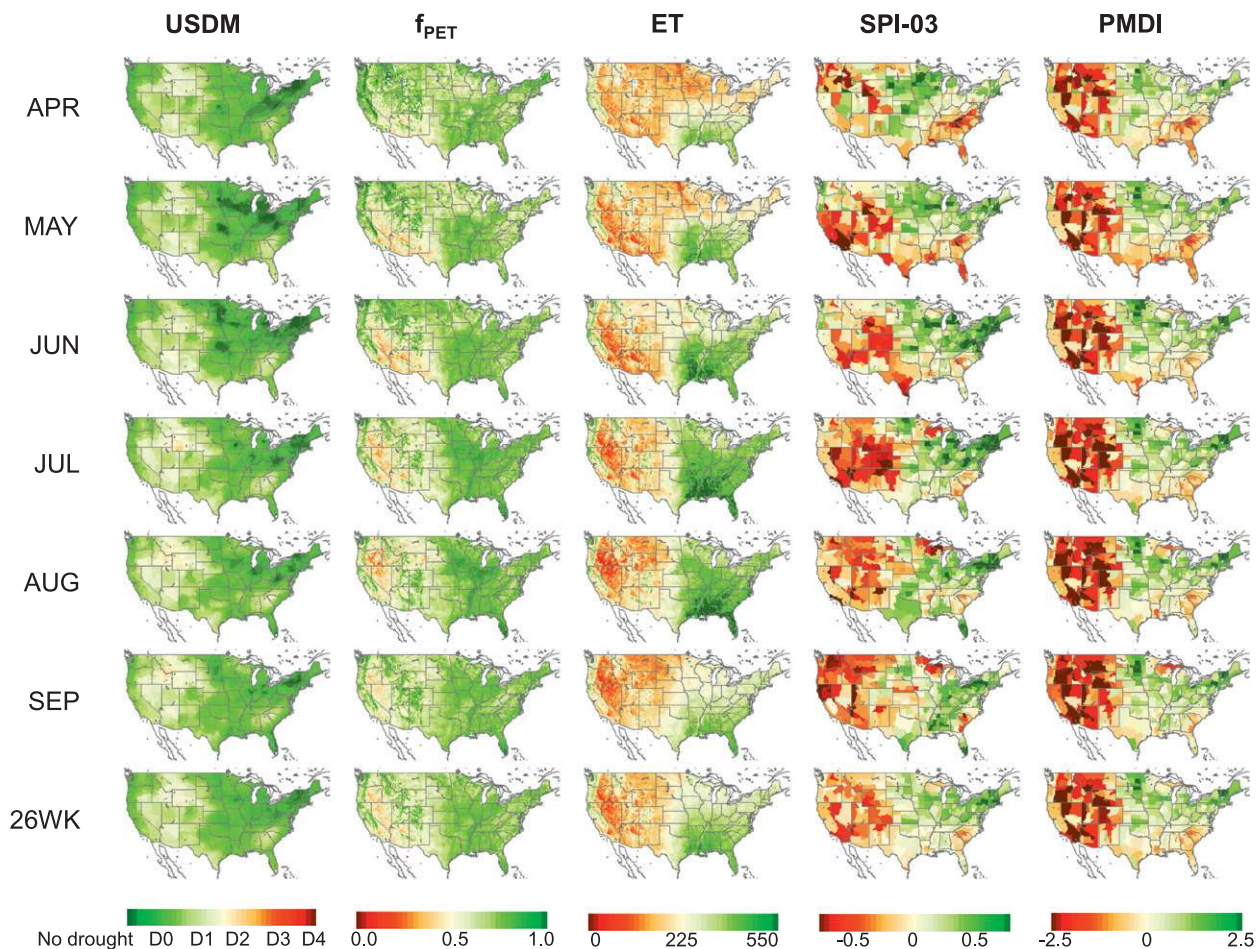
FIG. 2. Monthly and seasonally composited (26-week) maps of normal conditions for the USDM (–), f_{PET} (–), ET (W m^{-2}), SPI-3 (–), and PMDI (–) indices. Green indicates wetter conditions and red indicates drier conditions.

maps. This analysis demonstrates how spatial correlation strength varies from month to month and year to year based on climatic patterns.

A few caveats must be considered when interpreting correlations with the USDM classes. First, the USDM is not independent of the Palmer and SPI indices, as these are commonly used in the construction of USDM classifications. The ESI and ETI were not used in the USDM classification process over this period of record. Second, USDM drought classes incorporate information relevant to different kinds of drought over varying time scales, and we cannot expect a single indicator to agree perfectly with the USDM. For example, socioeconomic drought features in the USDM may indicate increased human demand for water rather than natural hydrological deficits. Finally, unlike the other indices, the USDM does not contain intrinsic information on wetter-than-average conditions. While the USDM should not be considered the absolute metric of "truth" in drought

monitoring, these comparisons give us insight as to how various indices can be most effectively used to inform the drought classification process.

3. Drought index intercomparison

a. Climatological characteristics

Maps of monthly and seasonal (26-week composite) normal conditions and standard deviations computed for the 2000–09 period are shown in Figs. 2 and 3 for the USDM drought classifications—ALEXI f_{PET} and ET—and two standard precipitation-based drought indices (SPI-3 and PMDI), selected to exemplify a range in time scales and modeling approaches. These fields are used to normalize monthly and seasonal anomalies [Eq. (4)] and to convey information about relative product resolution, spatial smoothness–noise, temporal variability, and the hydrologic-state variables considered in each index.
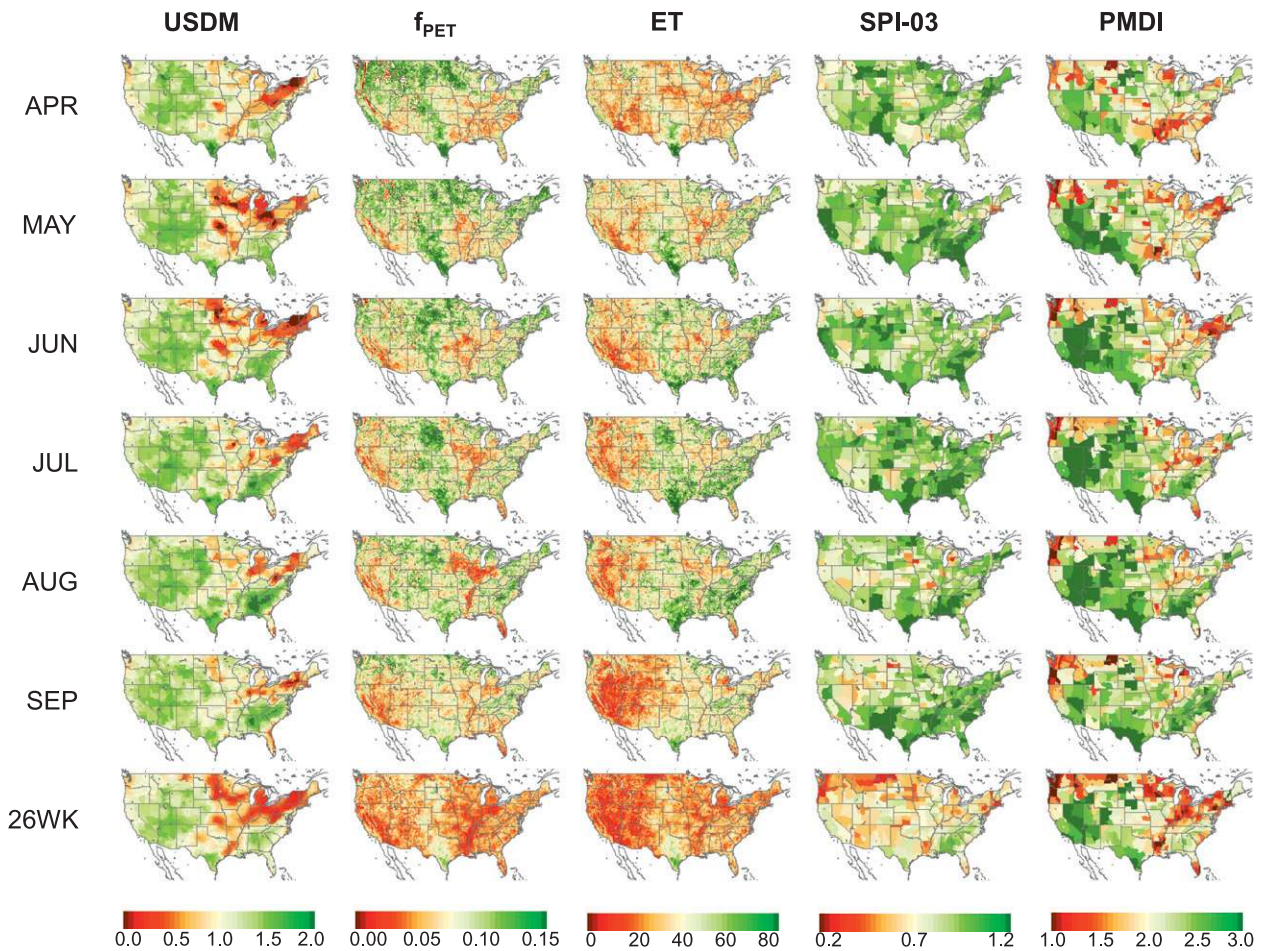
FIG. 3. As in Fig. 2, but for the temporal standard deviation. Red indicates lower variability.

The USDM normal fields (Fig. 2) indicate that the western United States has been generally classified as under drought of strength D1 or stronger over this 10-yr interval. The Midwest and Northeast were typically drought free or in D0, while the dry patch in the Southeast results primarily from the drought of 2007. Patterns in the f_{PET} normal maps are similar but not identical to those in the USDM. Seasonal discrepancies between the f_{PET}, USDM, and precipitation indices highlight areas where f_{PET} provides unique information about water use, where ET is partially decoupled from monthly rainfall rates. In July and August, for example, high average f_{PET} along the Mississippi River basin reflects enhanced ET due to shallow water tables and a high density of irrigated land area (Hain 2010). Similarly, ET in the managed agricultural areas of the Corn Belt (from Nebraska to Ohio) is typically maintained near potential during these months. These moisture features are less pronounced in the clear-sky ET normals, which are more strongly correlated with the seasonal cycle in vegetation cover fraction. Normalization by PET

appears to accentuate the tie between f_{PET} and soil moisture conditions, reducing the response to seasonal variations in vegetation amount and available energy.

Spatial patterns in the precipitation index normals (SPI-3 and PMDI) resemble the USDM normals, in part because these indices were used in producing the USDM reports. The NCDC datasets show strong spatial variability, likely reflecting sparsity and nonrepresentativeness in the gauge data used to create these indices. Gauge coverage is particularly problematic within western climate divisions, where we see the strongest noise in Fig. 2. In contrast, the ET indices are relatively smooth even when aggregated to the climate division scale, because of denser spatial sampling afforded by the remote sensing inputs. PMDI normal values for 2000–09 are peaked toward dry conditions (red tones) because this period was drier, on average, than the calibration interval used by NCDC to normalize the Palmer indices (1931–90; see Fig. 1). These bias effects are mitigated in the intercomparison to a large extent by the recomputation of standardized anomalies with respect to normal and
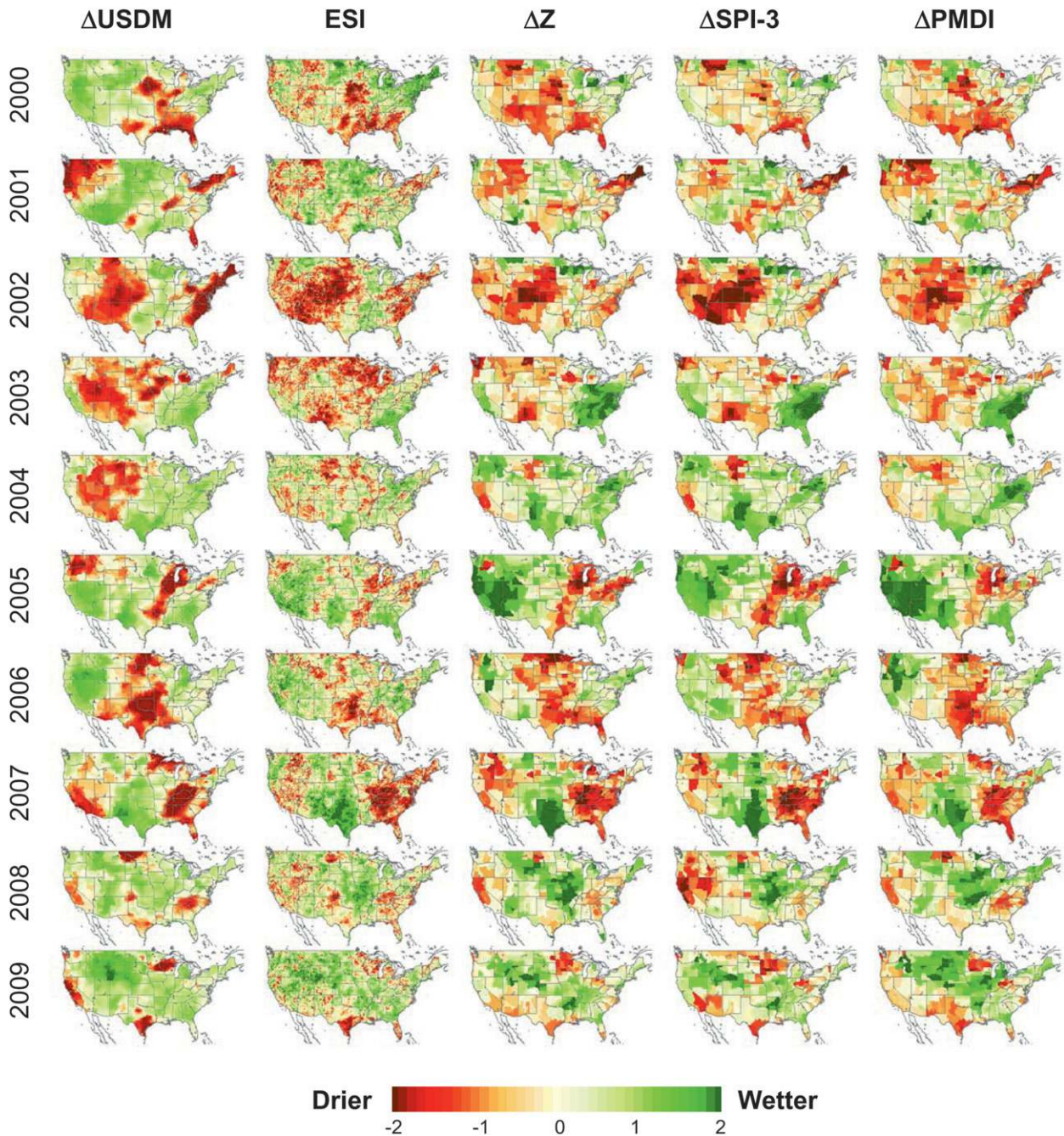
FIG. 4. Seasonal (26 week) anomalies in USDM, ESI, *Z*, SPI-3, and PMDI for 2000–09.

variability fields determined over a common interval (as described in section 2d).

The standard deviation fields in Fig. 3 convey additional insights about relative index behavior and information content, identifying regions where indices are more or less responsive to climatic drivers. The USDM drought classifications for 2000–09 were most variable in areas that experienced extreme drought during this period, including the western United States (2002–04), the Southeast (2007), and southern Texas (2009). The fraction of potential ET varied most strongly along the north–south midcontinent transition between the dry and humid temperate domains. Strong east–west gradients in vegetation cover and precipitation at this transition increase sensitivity in ET to annual climatic variability. In contrast, low variability in f_{PET} is observed over the
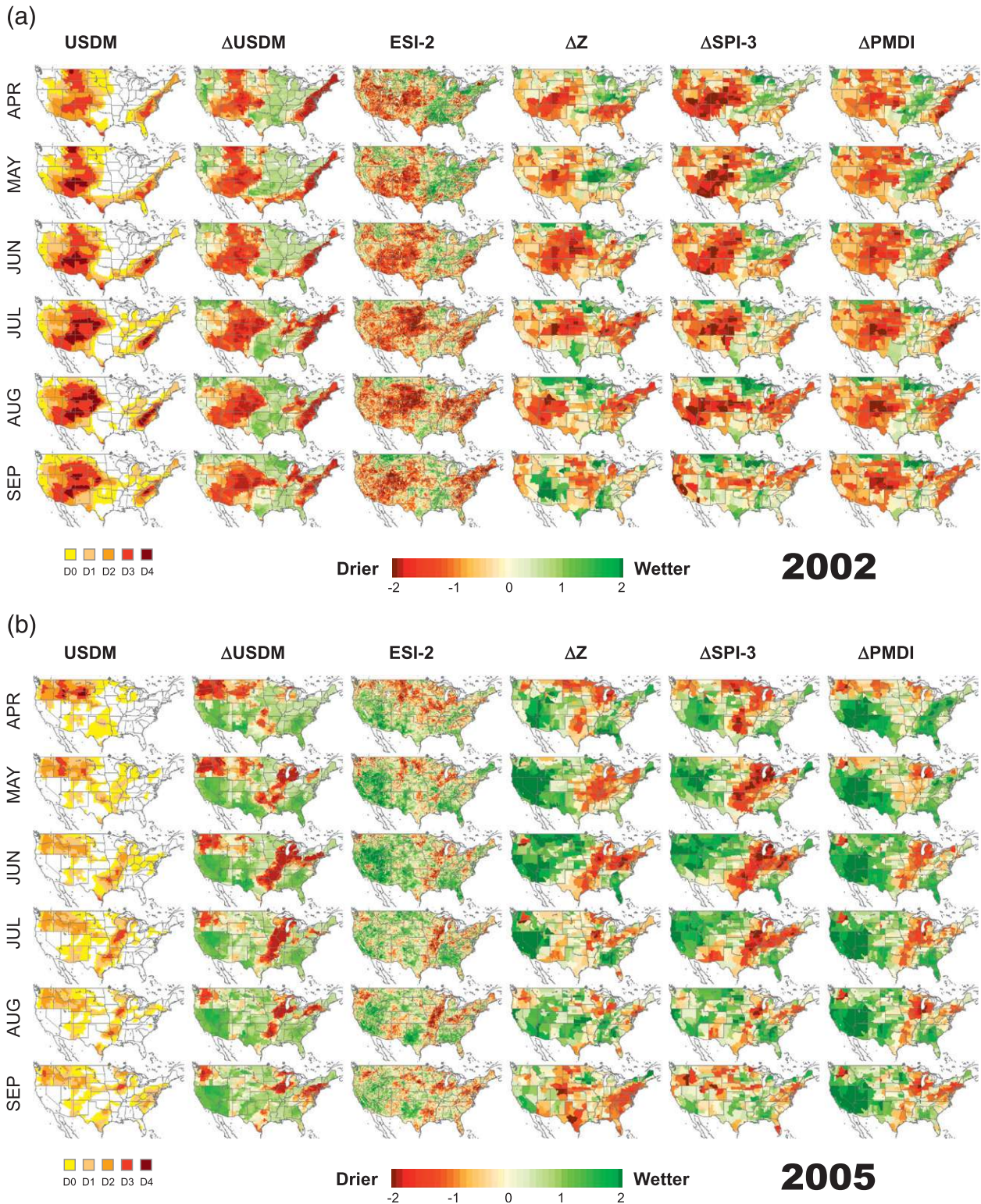
FIG. 5. (a) (second column, left to right) Monthly (Apr–Sep) standardized anomalies in the USDM drought classes (ΔUSDM), the ESI-2, the Palmer Z index (ΔZ), the 3-month SPI (ΔSPI-3), and the Palmer modified drought index (ΔPMDI) for 2002. (first column) The USDM drought classes for the week closest to the end of each month. (b) As in (a), but for 2005. (c) As in (a), but for 2007. (d) As in (a), but for 2009.
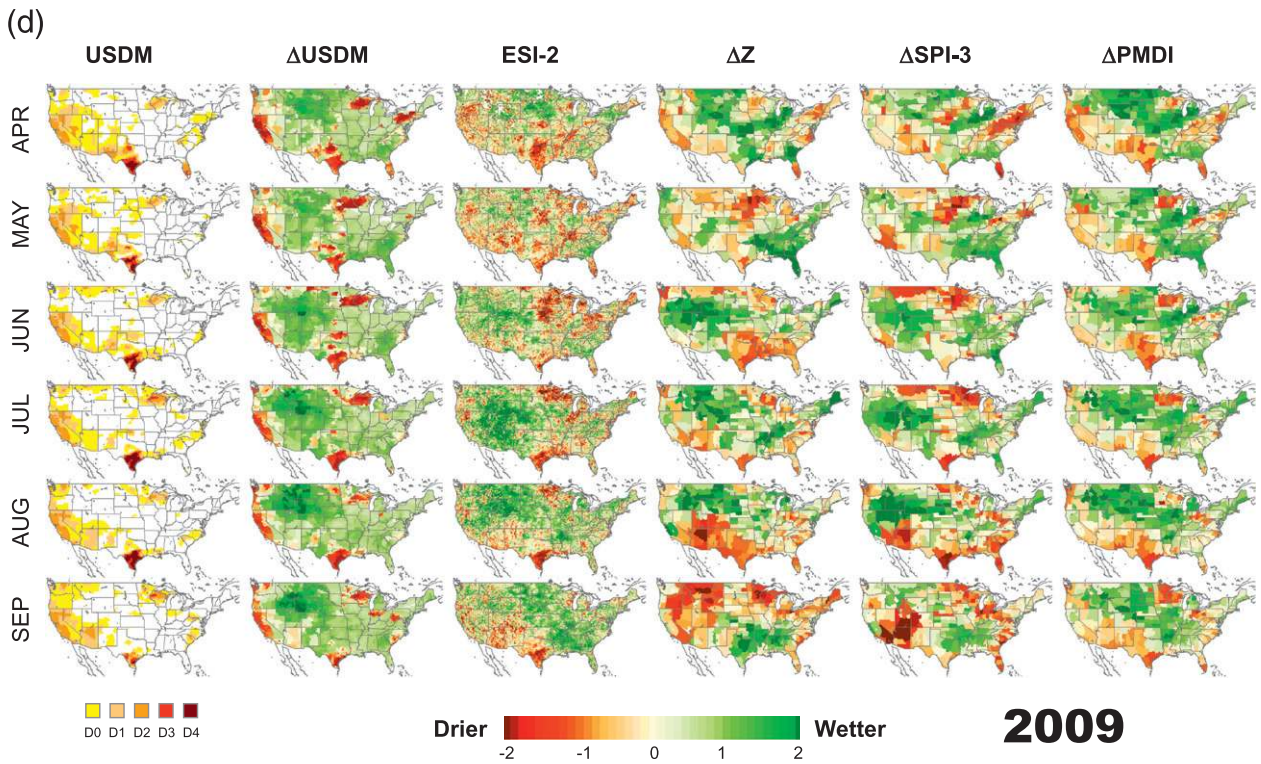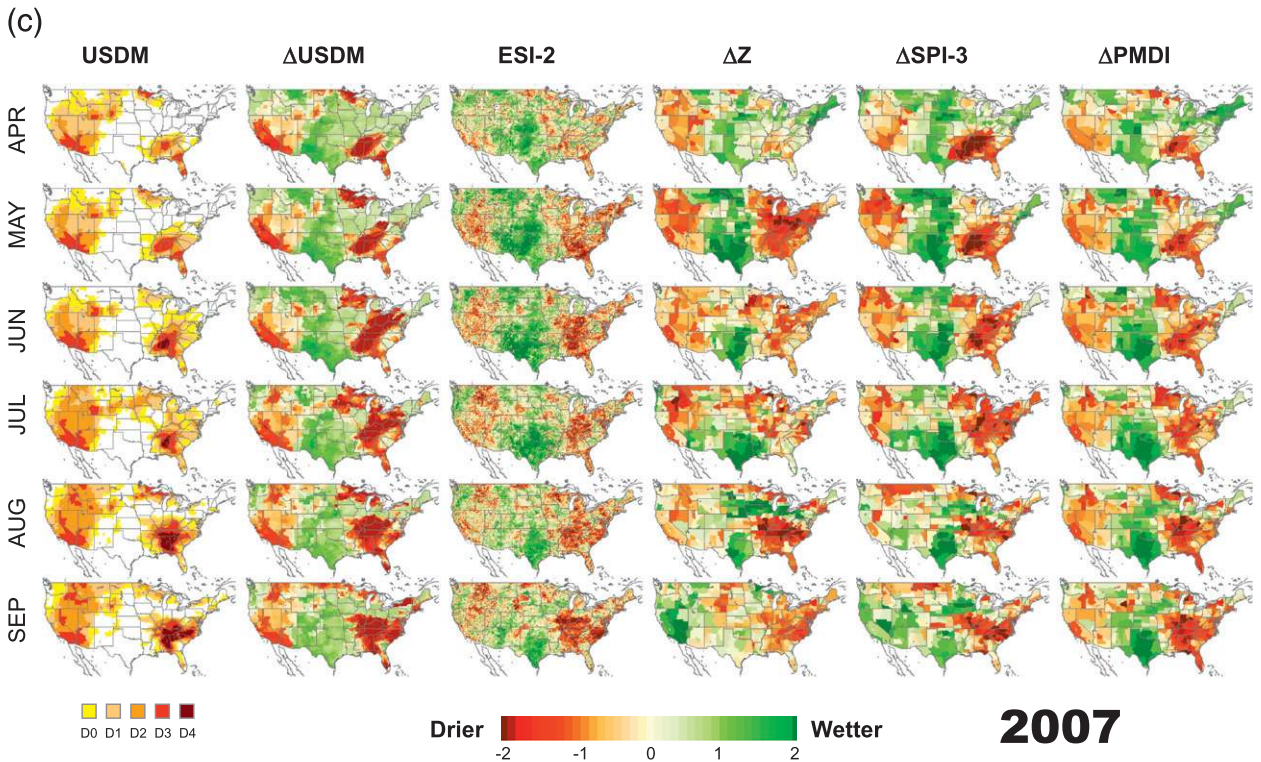
FIG. 5. (*Continued*)

Mississippi River basin, where riparian vegetation has access to shallow groundwater. Similar low variability features over Indiana, Ohio, and Florida also correspond to regions of shallow or inundated water table (Miguez-Macho et al. 2008). Temporal variance in f_{PET} may therefore be a useful indicator for mapping groundwater-dependent ecosystems.

Skewness, the third moment of the temporal distribution, was also assessed for each index. Skewness in f_{PET} and ET exhibited over this 10-yr period is generally low, with values between −1 and 1. The USDM shows stronger skew toward dry conditions, particularly in the East, where values exceeding 2 are observed. These are areas that tended to be drought free during this period and therefore strongly peaked at the "wet" end of the USDM class distribution (no drought). This skewness will degrade temporal and spatial correlations with other indices to some extent in the eastern United States, but it does not negate the general conclusions drawn from the intercomparison.

b. Seasonal and monthly drought patterns

Figure 4 compares annual patterns in drought over CONUS as represented by the USDM, ESI-2, Z, SPI-3, and PMDI indices for 2000–09. These maps show standardized anomalies computed for 26-week composites associated with the nominal growing season in the United States (April–September). ETI maps (not shown) are similar to the ESI but with lower interindex agreement (see section 3c). These figures demonstrate the diversity of information provided by different drought indicators, highlighting the complexity of developing a unified drought representation at the continental scale.

Drought features in the USDM are generally reflected in one or more of the other indices but to varying degrees depending on drought type and time scale. An exception is the multiyear hydrologic drought in the western United States in 2004, which is not well delineated by any of the shorter-term indices shown in Fig. 4 and only marginally captured in the longer-term PMDI and PHDI. In general, the ESI reproduces patterns evident in the precipitation indices, indicating the value of the LST signal as a surface moisture proxy. For example, the thermal band inputs to ALEXI capture the major drought events occurring in 2002 and 2007, even in the eastern United States, where there is dense vegetation cover midseason and little exposure of the dry soil surface. This is a part of CONUS, where standard soil moisture retrievals based on passive microwave remote sensing tend to lose sensitivity because of strong attenuation of the soil signal by water contained in the dense vegetation canopy. In the thermal band, however, the moisture deficit signal is strong—vegetation stress and soil moisture depletion in the

surface skin contribute to elevated canopy and soil components of the composite surface radiometric temperature.

Monthly index anomalies are shown in Fig. 5 for a few years with distinctive drought patterns. Here, an 8-week (two months) ESI compositing interval is used to maximize agreement with other indices while preserving month-to-month variability. The ESI reasonably tracks the time evolution of D3 and D4 drought patterns recorded in the USDM during 2002 and 2007 without significant lag (Figs. 5a and 5c). In some cases, USDM hotspots are better localized in the ESI than in the NCDC precipitation indices, because of the higher spatial resolution provided by the GOES LST inputs to ALEXI. Beginning in May 2005, for example, an unusual band of severe drought was established, extending from Illinois southwestward into Texas (Fig. 5b). A series of tropical storms in June–August (Arlene, Dennis, and Katrina) tracked east of the Mississippi River, confining the drought to this narrow band. The band was bifurcated by September, but drought in the northern and southern segments lingered into 2006. The ESI fields reproduce the development of this band of drought with reasonable spatial and temporal response to monthly precipitation patterns.

Some issues remain in the ESI processing stream, primarily in the area of incomplete archive and cloud clearing. In May and June of 2009, for example, the exceptional drought in Texas is not strongly identified in ESI-2, and there are extraneous drought signals that are not present in the other indices (Fig. 5d). These months had several extended periods with missing input data required to produce the ESI, and therefore the sampling in the composites was relatively poor. This exacerbates the effects of noise due to cloudy pixels undetected by the cloud screen, which tend to be averaged out when the daily sampling is more complete. Techniques for improving sampling in the ALEXI processing system are in development (see section 4).

c. Statistical intercomparisons

1) TEMPORAL CORRELATION ANALYSES

With the anomaly datasets we can determine how similarly the indices rank moisture conditions in time as a function of location across the CONUS domain. Maps describing the temporal similarity between the USDM and each of the drought indices considered in the intercomparison, in terms of linear correlation in monthly climate-division-based ranking of moisture conditions, are shown in Fig. 6, with domain-averaged correlation coefficients ($\langle r \rangle$) for all the index pairs listed in Table 2. Excluding autocorrelation effects, correlations of magnitude greater than 0.33 are statistically significant at $p = 0.01$.
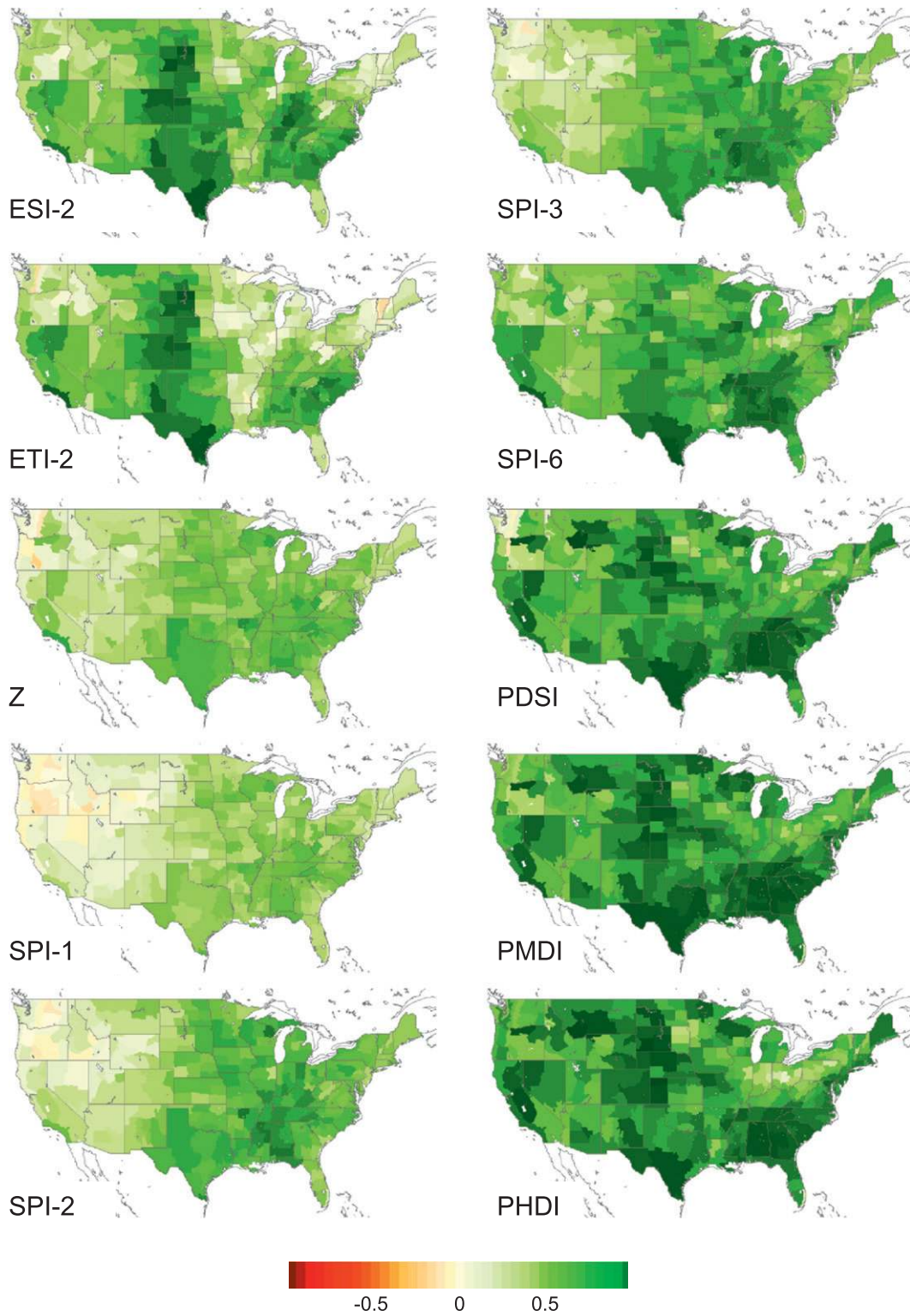
FIG. 6. Coefficient of temporal correlation between monthly maps of USDM anomalies and other drought indices included in the intercomparison for 2000–09.

TABLE 2. Average temporal correlation coefficient in pixel-based correlations of indices at monthly time steps. Bold values indicate the highest correlation for each index in a given column.

	ESI-2	ETI-2	ΔZ	ΔSPI-1	ΔSPI-2	ΔSPI-3	ΔSPI-6	ΔPDSI	ΔPMDI	ΔPHDI
ΔUSDM	0.536	0.477	0.416	0.282	0.434	0.508	0.603	0.664	**0.705**	0.698
ESI-2		**0.855**	0.425	0.282	0.485	0.544	0.547	0.564	0.591	0.560
ETI-2	**0.855**		0.332	0.213	0.417	0.491	0.495	0.491	0.517	0.497
ΔZ				**0.894**	0.752	0.679	0.562	0.641	0.637	0.534
ΔSPI-1			**0.894**		0.706	0.580	0.419	0.447	0.439	0.341
ΔSPI-2						**0.827**	0.598	0.585	0.598	0.497
ΔSPI-3					**0.827**		0.737	0.663	0.691	0.602
ΔSPI-6								0.764	**0.814**	0.776
ΔPDSI									**0.941**	0.905
ΔPMDI										**0.961**

Of the indices considered here, the PMDI and PHDI are most similar to the USDM in their temporal ranking of moisture conditions ($\langle r \rangle = 0.70$). This is in part because these indices are used in the construction of the USDM and therefore are not independent estimators of drought conditions. In addition, these indicators are relatively conservative, with a longer time-scale response to precipitation events more similar to that of the USDM, which typically does not change at the county level by more than one drought class between weekly reports.

In comparison with the USDM, the TIR-based ESI-2 yields higher average temporal correlations ($\langle r \rangle = 0.53$) than do the precipitation indices of shorter or comparable time scale (Z and SPI-1 to SPI-3, with $\langle r \rangle = 0.28–0.51$). In fact, in the northwestern United States, these short-term precipitation indices show a weakly negative correlation with USDM rankings. Shukla and Wood (2008) caution against using short-term SPIs in the U.S. Drought Monitor, noting that hydrologic delays in snowpack-forming regions can cause these indices to become desynchronized from land surface moisture conditions. In addition, SPI-1, SPI-2, and SPI-3 show weak correlations with the USDM in the southwestern United States. Wu et al. (2007) demonstrate that short-time-scale SPIs tend to have nonnormal temporal distributions in arid climates where precipitation distribution functions are highly skewed, peaking toward the no-rain case. In these situations, the 3-month SPI will tend to underpredict the severity and frequency of drought events, whereas the 6-month SPI shows more reasonable performance. This is consistent with the results in Fig. 6, which indicate that the SPI-6 is more highly correlated with the USDM in the western United States than is the SPI-3.

The ESI-2 does not exhibit the strong east–west dissimilarity in agreement with the USDM seen in SPI products of comparable time scale. The strongest correlations between the ESI and the USDM are observed over the Great Plains and in the southeastern United States. These are areas identified by Karnieli et al. (2010) where LST and NDVI tend to be anticorrelated, indicating moisture-limiting (as opposed to energy limiting) vegetation growth conditions. ET will be most sensitive to changing subsurface moisture conditions in these areas, and therefore anomalies should be indicative of drought. These are also regions where f_{PET} shows the highest temporal variability (Fig. 3). Reduced correlations between USDM and ESI are found along the Mississippi River basin, where shallow water tables and intensive irrigation tend to decouple ET rates from precipitation to some extent. The ESI also shows lower correlations with the USDM over the Everglades in south Florida. Here, the land surface is largely inundated with water over much of the year, and ET variations at the seasonal scale may be more related to climatic variability than to moisture availability. Lower correlations are also found in the northern states where, particularly in the early spring, ET is driven more by radiation and climate and is less tightly coupled with moisture/drought. In addition, the probability of cloud cover is higher in the northern United States (Hahn and Warren 2007), resulting in less frequent sampling of LST and greater uncertainty in the TIR-based satellite indices. In most CONUS climate divisions, the ESI is more strongly correlated with USDM drought classes than are ET anomalies (ETI-2).

Maps of coefficients of temporal correlation with the ESI-2 are shown in Fig. 7, with domain-averaged values also given in Table 2. The ESI shows best temporal agreement with the PMDI, suggesting that the remotely sensed ET estimates effectively integrate moisture conditions over time scales of several months. Agreement is strongest in hot spots of drought activity over that decade: in the southeast, the southwest, and in Texas. Good agreement is also found along the Great Plains, where the ESI has demonstrated enhanced sensitivity to precipitation amount.
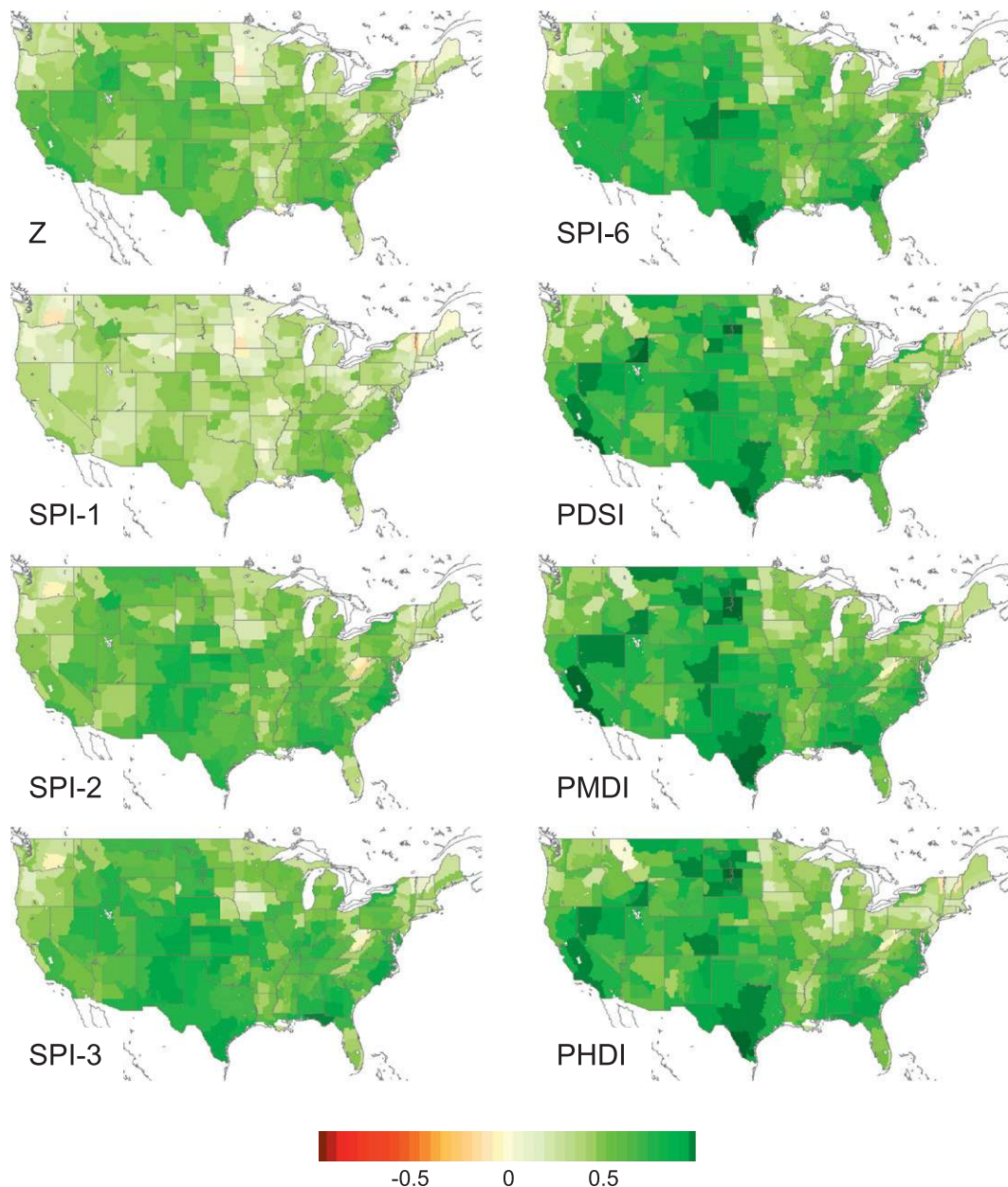
FIG. 7. As in Fig. 6, but between ESI-2 and other drought indices.

2) SPATIAL CORRELATION ANALYSES

With these datasets we can also examine the spatial similarity between maps of index anomalies and determine how this similarity evolves with time. Figure 8a shows yearly averaged coefficients of spatial correlation computed between monthly maps of USDM drought class anomalies and ESI-2, ETI-2, and the other drought indices in Table 1. Coherent year-to-year variability in index agreement is apparent. All indices show the weakest correlations in 2004 during the long-term hydrologic

drought event in the western United States, which was captured only by indices with time constants exceeding one year. The highest correlations are obtained in 2007, when there was a strong contrast in moisture conditions across CONUS. On average over all years, the spatial correlation of the ESI-2 with the USDM ranks between that of the SPI-3 and the SPI-6. ETI-2 correlations are consistently lower than those of ESI-2 by 0.05, on average.

Monthly average spatial correlations with USDM are plotted versus day of year in Fig. 8b to study the seasonal evolution in index agreement. At the monthly time scale,
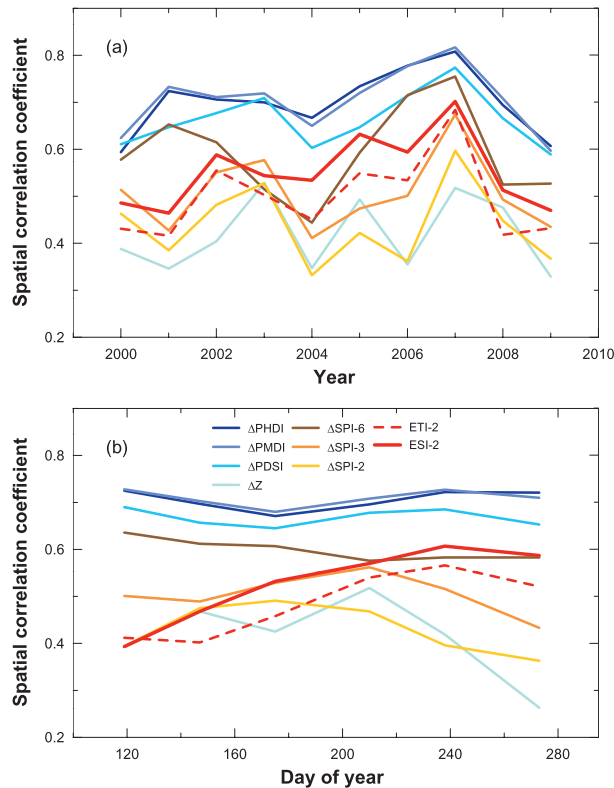
FIG. 8. CONUS-average coefficient of spatial correlation between monthly maps (April–September, 2000–09) of USDM anomalies and anomalies in other drought indices included in the intercomparison averaged by (a) year and (b) day of year.

spatial patterns in the USDM anomalies most closely resemble those in the longer-term indices: the PHDI, PMDI, PDSI, and SPI-6. The PHDI and PMDI show similar levels of agreement with the USDM, with correlations that are relatively uniform over the growing season. The modifications to the Palmer drought index algorithm implemented in the PMDI improve correlation with the USDM by 0.04, on average, in comparison with the standard PDSI. SPI-6 and ESI-2 rank next in terms of spatial similarity with the USDM, yielding a similar correlation, on average, past midseason. Correlations between ESI-2 and USDM are weakest in April and May. This may be partly due to poor temporal sampling in the ESI because of increased snow and cloud cover in the early spring. However, spatial similarity with ESI-2 increases steadily throughout the season as evaporative fluxes become increasingly moisture limited. In contrast, correlations between the short-term precipitation indices (Z, SPI-2, SPI-3) and the USDM and other indices tend to degrade in August and September. In several years (2002, 2006, 2007, and 2009), late-season rainfall or deficits in these months had little impact on

drought patterns that had developed during the growing season (see monthly maps in Fig. 5).

3) IMPACT OF ET COMPOSITING INTERVAL

The impact of compositing interval applied to the remotely sensed ET indices has been evaluated in terms of improvements in spatial and temporal correlation with respect to the suite of precipitation indices considered here. Figure 9 shows average spatial and temporal correlation coefficients for both the ESI and ETI in comparison with the USDM and other indices as a function of compositing interval, sampled at 2, 4, 8, and 12 weeks.

Both spatially and temporally, agreement in ranking between the ET indices and the USDM, PMDI, PHDI, PDSI, and SPI-6 improves with increasing ET-compositing interval, reaching a plateau at approximately eight weeks. For the shorter-term indices, the SPI-2 (2-month composite) is best correlated with the 4-week ET composites and SPI-3 with the 8-week ET composites. In other words, each SPI product agreed best with an ET index composited over an interval 4 weeks shorter than the SPI integration time scale. This suggests that evapotranspiration, as a physical process, integrates over a longer period than the equivalent precipitation interval—that is, it retains some memory of moisture conditions prior to the composite interval. The Z index is best correlated with the 2-week ET composites. The 1-week ET composites typically do not have full domain coverage because of cloud cover and show low correlations with all indices; therefore, they may have a limited utility for drought monitoring. In contrast, the 4- and 12-week composites may be most useful for USDM classifications, bracketing a range in drought time scales. A complete analysis using full-year datasets for each index is required to refine these recommendations for year-round monitoring.

The comparison of spatial and temporal correlation coefficients in Fig. 9 further demonstrates that, according to these metrics, anomalies in f_{PET} (ESI) are more strongly correlated with the other indices than are anomalies in ET (ETI) by approximately 0.05–0.10. Again, this is likely because by normalizing by PET, there is better isolation of variations in ET due to atmospheric demand and radiation load—factors not directly related to soil moisture conditions.

4. Discussion

Based on these results, we can draw some general conclusions regarding the relative strengths and weaknesses in the ESI approach to drought monitoring in comparison with standard drought metrics currently in operational use. The ESI provides unique information
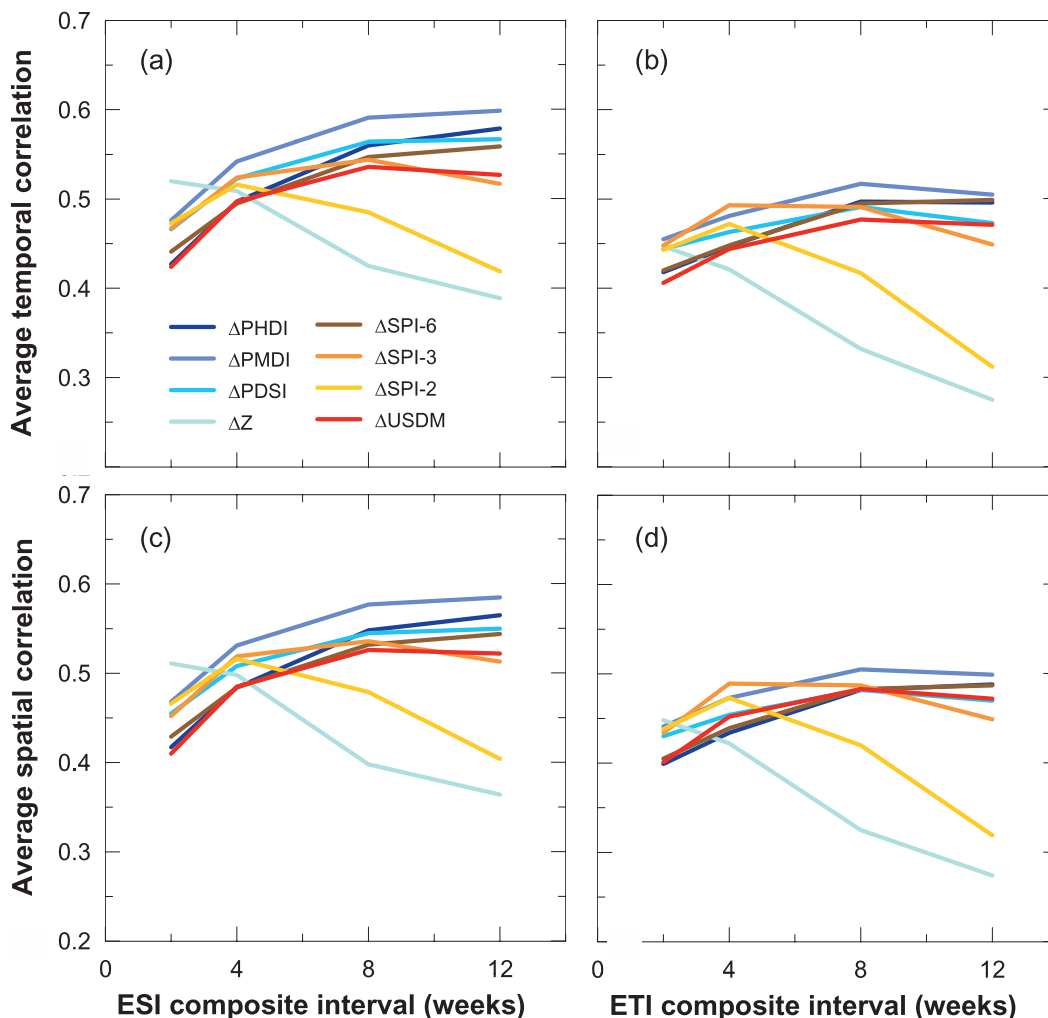
FIG. 9. CONUS-average coefficient of (top) temporal correlation and (bottom) time-average coefficient of spatial correlation between (left) ESI and (right) ETI and other drought indices included in the intercomparison as a function of ET index compositing interval.

not reflected in precipitation-based indices; however, because of its reliance on thermal remote sensing, it does suffer from sampling issues that add noise to regional assessments.

Remotely sensed ET and f_{PET} estimates include effects of artificial controls on water supply (e.g., irrigation, dams and diversions, interbasin water transfers, among others) that are decoupled from natural rainfall and streamflow patterns. Impacts of rainfall deficits on phreatophytic vegetation may also be locally mitigated by access to shallow groundwater, which also has a signature in the remotely sensed ET. Therefore, the ESI and ETI provide unique diagnostic information about actual stress that is not easily derived from precipitation data or hydrologic modeling without detailed information about management practices or water table distribution. In comparison to precipitation indices, we can obtain

information on where stress is being relieved by active water management or other nonprecipitation water inputs.

The focus on consumptive water use rather than water supply is also unique and builds in response to meteorological drivers (such as insolation, atmospheric humidity, and wind speed) as well as biophysical properties (such as plant water-use efficiency). Soil moisture will be lost from the system at different rates depending on these factors—for example, the so-called flash drought events, where prolonged hot, dry, and windy conditions lead to rapid water loss and the potential for catastrophic crop yield loss. Such events have caused great economic damage in the United States but are difficult to detect and explain using standard meteorological indices.

Some of the small-scale and diffuse structure evident in the ESI maps in Figs. 4 and 5 is likely noise related,

primarily because of incomplete cloud clearing. Improvements to the ALEXI preprocessing infrastructure, including the implementation of redundant input data streams and improved cloud masks, are underway and should help to reduce noise in future reprocessing of the ESI archive. However, dependence on clear-sky conditions required for thermal band LST retrieval necessarily places a physical limitation (related to cloud climatology) on the frequency of sampling achievable with the ALEXI ET algorithm. While a cloud gap-filling algorithm has been developed to generate time-continuous ET fields (Anderson et al. 2007b), gap-filled values are not independent samples of moisture conditions and do not add significant value to ESI composites. Therefore, the optimal remote sensing approach may be a multiband solution, integrating thermal data with microwave-based soil moisture information, which can be obtained under clear or cloudy skies. Joint assimilation of both TIR f_{PET} and microwave soil moisture retrievals into a prognostic LSM would serve to maximize both spatial and temporal sampling of surface moisture conditions and would provide additional hydrologic information, such as runoff, streamflow, and groundwater recharge (Hain 2010).

At present, ALEXI execution is also constrained to snow-free regions, further limiting sampling during the winter and early spring in some regions. A TIR-based snow energy balance modeling component, adapted from the work of Kongoli and Bland (2000), is in development to facilitate year-round ALEXI coverage. This model will estimate both the latent heat flux of evaporation and melting–freezing and sublimation over snow cover and will therefore provide additional information regarding soil moisture inputs during the snowmelt transition period.

5. Conclusions

An intercomparison was conducted between drought indices based on remotely sensed evapotranspiration, ground observations of rainfall (e.g., the Palmer indices and the standardized precipitation index), and drought classifications reported in the USDM from 2000 to 2009. Spatial distributions in ESI, representing anomalies in the ratio of actual to potential ET (f_{PET}), were found to correlate well with patterns in precipitation-based indices and in the USDM, responding to rainfall events at monthly time scales. Both spatially and temporally, agreement between the USDM drought classes and 2-month ESI composites ranked between USDM correlations with 3- and 6-month SPI products, suggesting that ET as a physical process has significant integrative memory of prior moisture conditions. Of the drought indicators examined here, the ESI exhibits spatial and temporal behavior most similar to that of the PMDI. In general, f_{PET} anomalies were better correlated with the other drought classifications than were anomalies in ET itself, indicating that normalization by PET results in a better surface moisture proxy.

Because the USDM cannot be considered a metric of absolute truth in drought mapping, this study is not intended as an assessment of index performance but rather a study of what types and time scales of information appear to be most correlated with subjective expert-interpreted drought severity delineations that have been made in the past. Such analyses may help to inform the development of objective drought indicator blends. In some cases, low correlations might in fact identify regions of unique contribution by a particular indicator, highlighting information not currently conveyed in the USDM. For example, lower ESI correlations are found in areas where groundwater is contributing (naturally or through irrigation) to the surface moisture supply, and evaporative fluxes are expected to be coupled to precipitation rates only over long time scales. Such impacts on drought resilience are difficult to model prognostically, but they have significant ramifications for yield forecasting and decision making. Because precipitation is not used in the construction of the ESI, this index provides an independent assessment of drought conditions and will have particular utility for real-time monitoring in regions with sparse rainfall data or significant delays in meteorological reporting.

Future analyses of the ESI will include comparisons with drought indices based on ET, soil moisture, and surface runoff estimates from the NLDAS land surface modeling system that are currently used in the National Centers for Environmental Prediction (NCEP) North American Drought Briefing and with other remote sensing drought indices, such as the vegetation heath index (VHI; Kogan 1997) and the vegetation drought response index (VegDRI; Brown et al. 2008). The domain of the ALEXI application is being expanded to include North and South America (approximately −60 to 60° latitude) using GOES data. Other domains are being established over southern Europe, the Middle East, and the African continent using land surface products from the European Meteosat Second Generation (MSG) satellites. A longer-term goal of global ESI coverage (excluding the poles) can be obtained with the current international system of geostationary satellites. Finally, work is underway to incorporate a snow module in ALEXI so that it can be applied year-round.

REFERENCES

Alley, W. M., 1984: The Palmer drought severity index: Limitations and assumptions. *J. Climate Appl. Meteor.,* **23,** 1100–1109.

Anderson, M. C., J. M. Norman, G. R. Diak, W. P. Kustas, and J. R. Mecikalski, 1997: A two-source time-integrated model for estimating surface fluxes using thermal infrared remote sensing. *Remote Sens. Environ.,* **60,** 195–216.

——, W. P. Kustas, and J. M. Norman, 2007a: Upscaling flux observations from local to continental scales using thermal remote sensing. *Agron. J.,* **99,** 240–254.

——, J. M. Norman, J. R. Mecikalski, J. P. Otkin, and W. P. Kustas, 2007b: A climatological study of evapotranspiration and moisture stress across the continental U.S. based on thermal remote sensing: 1. Model formulation. *J. Geophys. Res.,* **112,** D10117, doi:10.1029/2006JD007506.

——, ——, ——, ——, and ——, 2007c: A climatological study of evapotranspiration and moisture stress across the continental U.S. based on thermal remote sensing: 2. Surface moisture climatology. *J. Geophys. Res.,* **112,** D11112, doi:10.1029/2006JD007507.

Brown, J. F., B. D. Wardlow, T. Tadesse, M. J. Hayes, and B. C. Reed, 2008: The vegetation drought response index (VegDRI): A new integrated approach for monitoring drought stress in vegetation. *GIScience Remote Sens.,* **45,** 16–46.

Edwards, D. C., and T. B. McKee, 1997: Characteristics of 20th century drought in the United States at multiple time scales. Colorado State University Climatology Rep. 97-2, 174 pp.

Guttman, N. B., 1997: Comparing the Palmer drought index and the standardized precipitation index. *J. Amer. Water Resour. Assoc.,* **35,** 113–121.

——, and R. G. Quayle, 1996: A historical perspective of U.S. climate divisions. *Bull. Amer. Meteor. Soc.,* **77,** 293–303.

Hahn, C. J., and S. G. Warren, 2007: A gridded climatology of clouds over land (1971-96) and ocean (1954-97) from surface observations worldwide. Carbon Dioxide Information Analysis Center Rep. NDP-026E, 71 pp.

Hain, C. R., 2010: Developing a dual assimilation approach for thermal infrared and passive microwave soil moisture retrievals. Ph.D. thesis, Department of Atmospheric Science, University of Alabama, 200 pp.

Heddinghaus, T. R., and P. Sabol, 1991: A review of the Palmer drought severity index and where do we go from here? *Proc. Seventh Conf. on Applied Climatology,* Salt Lake City, UT, Amer. Meteor. Soc., 242–246.

Heim, R. R., 2002: A review of twentieth-century drought indices used in the United States. *Bull. Amer. Meteor. Soc.,* **83,** 1149–1165.

Huffman, G. J., and Coauthors, 2007: The TRMM Multisatellite Precipitation Analysis (TMPA): Quasi-global, multiyear, combined-sensor precipitation estimates at fine scales. *J. Hydrometeor.,* **8,** 38–55.

Joyce, R. J., J. E. Janowiak, P. A. Arkin, and P. Xie, 2004: CMORPH: A method that produces global precipitation estimates from passive microwave and infrared data at high spatial and temporal resolution. *J. Hydrometeor.,* **5,** 487–503.

Karl, T. R., 1983: Some spatial characteristics of drought duration in the United States. *J. Climate Appl. Meteor.,* **22,** 1356–1366.

Karnieli, A., N. Agam, R. T. Pinker, M. C. Anderson, M. L. Imhoff, G. G. Gutman, N. Panov, and A. Goldberg, 2010: Use of NDVI and land surface temperature for drought assessment: Merits and limitations. *J. Climate,* **23,** 618–633.

Knapp, K. R., 2008: Scientific data stewardship of International Satellite Cloud Climatology Project B1 global geostationary observations. *J. Appl. Remote Sens.,* **2,** 023548, doi:10.1117/1.3043461.

Kogan, F. N., 1997: Global drought watch from space. *Bull. Amer. Meteor. Soc.,* **78,** 621–636.

Kongoli, C. E., and W. L. Bland, 2000: Long-term snow depth simulations using a modified atmosphere-land exchange model. *Agric. For. Meteor.,* **104,** 273–287.

Kustas, W. P., and J. M. Norman, 1999: Evaluation of soil and vegetation heat flux predictions using a simple two-source model with radiometric temperatures for partial canopy cover. *Agric. For. Meteor.,* **94,** 13–29.

——, and ——, 2000: A two-source energy balance approach using directional radiometric temperature observations for sparse canopy covered surfaces. *Agron. J.,* **92,** 847–854.

——, G. R. Diak, and J. M. Norman, 2001: Time difference methods for monitoring regional scale heat fluxes with remote sensing. *Land Surface Hydrology, Meteorology, and Climate: Observations and Modeling,* V. Lakshmi, J. Albertson, and J. Schaake, Eds., Water Science and Application Series, Vol. 3, Amer. Geophys. Union, 15–29.

McEnery, J., J. Ingram, Q. Duan, T. Adams, and L. Anderson, 2005: NOAA's Advanced Hydrologic Prediction Service. *Bull. Amer. Meteor. Soc.,* **86,** 375–385.

McKee, T. B., N. J. Doesken, and J. Kleist, 1993: The relationship of drought frequency and duration to time scales. Preprints, *Eighth Conf. on Applied Climatology,* Anaheim, CA, Amer. Meteor. Soc., 179–184.

——, ——, and ——, 1995: Drought monitoring with multiple time scales. Preprints, *Ninth Conf. on Applied Climatology,* Dallas, TX, Amer. Meteor. Soc., 233–236.

McNaughton, K. G., and T. W. Spriggs, 1986: A mixed-layer model for regional evaporation. *Bound.-Layer Meteor.,* **74,** 262–288.

Mecikalski, J. M., G. R. Diak, M. C. Anderson, and J. M. Norman, 1999: Estimating fluxes on continental scales using remotely sensed data in an atmospheric–land exchange model. *J. Appl. Meteor.,* **38,** 1352–1369.

Miguez-Macho, G., H. Li, and Y. Fan, 2008: Simulated water table and soil moisture climatology over North America. *Bull. Amer. Meteor. Soc.,* **89,** 663–672.

Mitchell, K. E., and Coauthors, 2004: The multi-institution North American Land Data Assimilation System (NLDAS): Utilizing multiple GCIP products and partners in a continental distributed hydrological modeling system. *J. Geophys. Res.,* **190,** D07S90, doi:10.1029/2003JD003823.

Mo, K. C., 2008: Model-based drought indices over the United States. *J. Hydrometeor.,* **9,** 1212–1230.

Moran, M. S., 2003: Thermal infrared measurement as an indicator of plant ecosystem health. *Thermal Remote Sensing in Land Surface Processes,* D. A. Quattrochi and J. Luvall, Eds., Taylor and Francis, 257–282.

Norman, J. M., W. P. Kustas, and K. S. Humes, 1995: A two-source approach for estimating soil and vegetation energy fluxes from observations of directional radiometric surface temperature. *Agric. For. Meteor.,* **77,** 263–293.

——, and Coauthors, 2003: Remote sensing of surface energy fluxes at 10^1-m pixel resolutions. *Water Resour. Res.,* **39,** 1221, doi:10.1029/2002WR001775.

Palmer, W. C., 1965: Meteorological drought. U.S. Weather Bureau Rep., 65 pp.

Schaake, J. C., and Coauthors, 2004: An intercomparison of soil moisture fields in the North American Land Data Assimilation System (NLDAS). *J. Geophys. Res.,* **109,** D01S90, doi:10.1029/2002JD003309.

Shukla, S., and A. W. Wood, 2008: Use of a standardized runoff index for characterizing hydrologic drought. *Geophys. Res. Lett.,* **35,** L02405, doi:10.1029/2007GL032487.

Svoboda, M., and Coauthors, 2002: The drought monitor. *Bull. Amer. Meteor. Soc.,* **83,** 1181–1190.

Thornthwaite, C. W., 1948: An approach toward a rational classification of climate. *Geogr. Rev.,* **38,** 55–94.

Villarini, G., W. F. Krajewski, and J. A. Smith, 2009: New paradigm for statistical validation of satellite precipitation estimates: Application to a large sample of the TMPS 0.25° 3-hourly estimates over Oklahoma. *J. Geophys. Res.,* **114,** D12106, doi:10.1029/2008JD011475.

Wells, N., S. Goddard, and M. J. Hayes, 2004: A self-calibrating Palmer drought severity index. *J. Climate,* **17,** 2335–2351.

Wilhite, D. A., and M. H. Glantz, 1985: Understanding the drought phenomenon: The role of definitions. *Water Int.,* **10,** 111–120.

Wu, H., M. D. Svoboda, M. J. Hayes, D. A. Wilhite, and F. Wen, 2007: Appropriate application of the standardized precipitation index in arid locations and dry seasons. *Int. J. Climatol.,* **27,** 65–79.

Zeweldi, D. A., and M. Gebremichael, 2009: Evaluation of CMORPH precipitation products at fine space–time scales. *J. Hydrometeor.,* **10,** 300–307.